38th International Electric Vehicle Symposium and Exhibition (EVS38) Göteborg, Sweden, June 15-18, 2025

Impact of Energy Management in Alternative Vehicle Technologies according to Usage Profiles

A. Luciano[1], Miguel Campino [2,3], P. Baptista [2,3], G. O. Duarte [3,4]

[1]*António Luciano (correspondig author) Mechanical Engineering Department - Instituto Superior Técnico, Universidade de Lisboa, Av. Rovisco Pais, 1 - 1049-001 Lisboa – Portugal, antonio.luciano@tecnico.ulisboa.pt*

[2] *Mechanical Engineering Department - Instituto Superior Técnico, Universidade de Lisboa, Av. Rovisco Pais, 1 - 1049-001 Lisboa – Portugal*

[3] *IN+, Center for Innovation, Technology and Policy Research - Instituto Superior Técnico, Universidade de Lisboa, Av. Rovisco Pais, 1 - 1049-001, Lisboa*

[4] *Mechanical Engineering Department - Instituto Superior de Engenharia de Lisboa (ISEL), Rua Conselheiro Emídio Navarro, 1 – 1959-007 Lisboa, Portugal*

Executive Summary

The imperative to electrify the transportation sector underscores the need for understanding the energy management across propulsion technologies. Using in-house tools and AVL Cruise M, vehicle models were constructed to gather insights on different powertrain systems for sustainable transportation across different usage profiles. Megajoule per km values for representative routes in Lisbon were determined for human-driven and autonomous vehicles during and outside rush hour. For passenger transport, battery electric vehicles (BEVs) and fuel cell electric range extenders (FCEVRx) in charge-depleting mode showed the lowest consumption. For cargo transport, insights were gained on the effect of regenerative braking in fully loaded FCEVs, with frequent stops helping to offset reduced route fluidity, while BEVs exhibited similar behavior to passenger vehicles. Conclusions on automation potential indicated that heavier and more powerful car segments benefit most in energy reduction.

Keywords: Electric Vehicles, Fuel Cell Electric Vehicles, Modelling & Simulation, Energy Management, Consumer behavior

1 Introduction

Climate change, largely driven by human-generated greenhouse gas (GHG) emissions, is a critical global challenge with severe environmental, economic, and humanitarian impacts [1]. The Paris Agreement, signed by 196 nations at COP21, aims to limit global warming to below 2°C, ideally targeting 1.5°C above preindustrial levels. Every five years, nations submit Nationally Determined Contributions (NDCs) outlining their emissions reduction plans, with the next round due in 2025 for targets extending to 2035 [2]. While current policies have reduced the projected 2030 GHG emissions increase from 16% to 3%, this falls short of the IPCC's 1.5°C and 2°C targets. The IPCC notes that even with full implementation of current NDCs, substantial cuts — 28% for 2°C and 42% for 1.5°C — are required by 2030. Projections for 2035 show that current policies would result in GHG emissions exceeding 2°C and 1.5°C pathways by 36% and 55%, respectively, emphasizing the need for more ambitious policies to close the emissions gap [3]. Globally, the transportation sector was the

second largest contributor to GHG emissions in 2019, accounting for 15.05% of total emissions in CO_2 equivalent (CO_{2eq}) terms [4]. In 2021, in the EU, while recovering from the pandemic, the transport sector represented almost one-quarter of total GHG emissions, with road transport making up more than three-quarters of that. Cars were the largest contributor at 58.9%, followed by Heavy-Duty Trucks and Buses at 28%, Light-Duty Trucks at 11.8%, and motorcycles and other road transport at 1.3%. Notably, transportation is the only sector in the EU with consistently rising emissions relative to 1990 levels [5].

2 Adaptation of Technology to Mobility Patterns

Mobility patterns depict either individual movement phenomena or spatial functions influenced by human activity [6]. Understanding how this mobility patterns can be leveraged to adapt to new low-carbon technologies and maximize their benefits and best applications is a crucial step in the transition, providing insights in the deployment of infrastructure and optimization of grid management and EV charging scheduling [7, 8]. Vehicle typology is also something to consider its mobility usage. Each vehicle type should be correlated with distinct trip making behaviors, encompassing quantitative aspects like trip frequency, distance traveled and driving speed, as well as qualitative characteristics reflected in spatial-temporal trip patterns [9]. Studies on driving patterns have identified major vehicle activity contexts using Floating Car Data (FCD) and clustering algorithms, classifying vehicle types by usage behaviors [9]. These studies reveal significant differences in roadway usage, while other research has used machine learning models to analyze driving patterns in EVs, addressing power consumption challenges by enabling real time power estimation through classification models [10]. Further analysis links EV charging needs to driving patterns, revealing how mobility behaviors can inform charging infrastructure planning and optimize grid load by shifting demand to off-peak hours [11, 12]. Despite these insights, there is a gap in comprehensive studies assessing energy management systems across varied usage scenarios, such as private vehicles, taxis, long-distance commuters, freight transportation, and autonomous vehicles. The objective of this work aims to evaluate the energy and environmental impact per kilometer of real-world trips, focusing on traffic conditions (rush hour vs. non-rush hour) for passenger and cargo transportation.

3 Methodology

The method consists of two steps: (1) Data collection and driving cycle construction to gather and prepare information for creating a representative driving cycle; (2) Vehicle model development.

3.1 Data Collection and Driving Cycle Construction

The methodology begins by selecting representative routes, followed by data collection using a MATLAB function that formats origin and destination coordinates for API requests. The route data is processed into a matrix detailing time, speed, distance, and coordinates. API data enhance the route matrix with road types, speed limits, and elevation data. Refinements ensure smooth coordinate transitions and remove redundant traffic sign information. The driving cycle construction is drawn from [13], which begins by identifying stops (e.g., at traffic lights, crosswalks) and creating a vector to represent vehicle movement with randomness for variability in stop patterns. A matrix includes stop durations, target speeds (factoring in legal limits and conditions), and random" hard braking" events for obstacles. Using target speed and maneuver data, a second-by-second speed profile is built, adjusting for accelerations, decelerations, and stops. Distance covered is calculated each second, ensuring alignment with expected stopping and maneuver distances and speeds. For the creation of cycles for autonomous vehicles, it was assumed that the vehicle was a connected and autonomous vehicle (CAV), connected to the grid of traffic lights, thereby reducing significantly the need to stop.

3.1.1 **Usage Profiles**

This study considers two main vehicle usage scenarios: passenger transportation and cargo distribution. Passenger routes (A1, A2, B1 and B2) include autonomous or human-driven options while cargo routes (C1, C2 and C3) solely considers the human-driven scenario. Route characteristics are summarized in Table 1.

Table 1: Summary of Route Characteristics

Route	Case		Distance (km)	Trip Time (s)	Stop Time (s)	Nº Stops	Δhmáx (m)	$h_{initial}/h_{fimal}$ (m)
A1	HRH	Mean	7.5	1257.3	519.5	19.0	81.0	102/27
		std.		76.5	59.2	1.3	-	-
	HORH	Mean	6.3	1021.5	388.6	21.9	81.0	102/27
		std.		56.1	44.8	1.4	-	-
	ARH	Mean	7.5	639.6	16.8	5.0	81.0	102/27
		std.		12.9	6.4	0.9	-	-
	AORH	Mean	7.6	629.2	3.7	3.3	81.0	102/27
		std.		8.4	0.7	0.5	-	-
A2	HRH	Mean	7.3	3508.3	2471.1	72.6	81.0	27/102
		std.		140.8	145.7	3.6	-	-
	HORH	Mean	7.6	1265.6	516.3	18.5	81.0	27/102
		std.		65.9	56.5	2.6	-	-
	ARH	Mean	7.3	644.5	13.4	4.5	81.0	27/102
		std.		7.6	4.3	0.7	-	-
	AORH	Mean	7.8	649.0	3.3	2.8	81.0	27/102
		std.		10.7	1.1	0.6	-	-
B1	HRH	Mean	16.0	2681.9	1449.4	47.8	113.0	20/7
		std.		96.1	91.1	2.2	-	-
	HORH	Mean	16.5	1453.3	350.5	15.2	113.0	20/7
		std.		69.7	60.2	2.2	-	-
	ARH	Mean	17.1	1111.6	45.2	12.6	113.0	20/7
		std.		18.3	12.5	1.7	-	-
	AORH	Mean	17.4	1064.5	7.2	6.1	113.0	20/7
		std.		10.3	2.4	1.6	-	-
B2	HRH	Mean	18.9	2615.8	1285.6	40.4	112.0	7/20
		std.		134.4	128.4	1.9	-	-
	HORH	Mean	19.3	1535.5	315.3	13.4	112.0	7/20
		std.		64.7	57.6	1.2	-	-
	ARH	Mean	16.2	1564.6	13.6	4.5	112.0	7/20
		std.		13.9	6.7	1.5	-	-
	AORH	Mean	16.5	1534.5	2.6	2.4	112.0	7/20
		std.		19.7	1.1	0.9	-	-
C1	HRH	Mean	7.0	3065.8	2149.6	66.3	72.0	72/43
		std.		94.1	86.6	3.0	-	-
	HORH	Mean	7.6	1165.8	438.7	17.3	72.0	72/43
		std.		74.1	63.3	1.9	-	-
C2	HRH	Route		5219.0	3608.0	137.0		
		Mean	10.2	208.8	144.3	5.5	97.0	43/98
		std.		2.5	30.1	1.2	-	-
	HORH	Route		2153.0	699.0	62.0		
		Mean	11.1	86.1	28.0	2.5	97.0	43/98
		std.		4.4	16.6	0.5	-	-
C3	HRH	Route		1150.0	125.5	44.0		
		Mean	7.1	76.7	26.7	2.9	75.0	13/14
		std.		6.6	23.8	1.4	-	-
	HORH	Route		905.0	164.5	35.0		
		Mean	7.6	60.3	8.4	2.3	75.0	13/14
		std.		4.9	10.3	0.4	-	-

As described in table 1, seven base cases are considered: three for cargo and four for passengers. For simplicity, each case is coded with 'H' or 'A' to indicate whether the vehicle is human-driven or autonomous, followed by 'RH' for rush hour or 'ORH' for off-peak hours, depending on the specific usage profile being analyzed. Passenger routes simulate touristic and commute trips in Lisbon, following [14]. Cargo routes are based on urban and sub-urban logistics from [15].

3.2 Vehicle Model Development

Four vehicle models, an L6e, C-Segment, Light duty van and E-segment were developed based on real life counterparts of the same segment emphasizing the availability of technical data and the vehicles' prevalence in the Portuguese market. Vehicle models were built in AVL Cruise M, leveraging default models and generators for parameterizing components, as well as approximations when publicly data was unavailable. The aerodynamic characteristics of the vehicles were approximated by the model with the input of the frontal area and the drag coefficient. According to [16] the frontal area of a vehicle can be estimated according to equation 1.

$$A_f = -1.23069 + 0.00011 m_v \times W \times H - 0.05398(W \times H)^2 \quad (1)$$

Where A_f is the estimated frontal area (m²), m_v is the vehicle mass (kg), W is the vehicle width (m), and H is the vehicle height (m). Motor torque-rpm curves were produced through the maximum torque and using the sustaining constant torque and constant power areas of the curve from available data. The Light duty-van and C- segment efficiency maps were based on [17]. The E-segment motor curve and efficiency map were drawn from [18]. For the L6e, an efficiency map produced by the AVL Cruise M generator was adapted. To evaluate the mass impact of the technology used, specific assumptions about power-to-mass ratios were applied regarding the fuel cells. This approach similar to the one used in [19] allowed for a more detailed analysis of how technology affects mass increases in the models. The data for the fuel cell models mass and power were sourced from [20]. The data showed a clear nonlinear behavior, and therefore a power trendline on the form $y = ax^b$ for a better fit on the values. For the hydrogen tanks, a linear approximation between the hydrogen mass and the tank mass was performed using data from [21]. Those relations are present in Equations 2 and 3. A general equation for the BEV battery weight as a function of power, shown in Equation 4, was also adapted from [19]. Equation 5 provides a relation based on [22] for the low capacity, high power density battery of the FCEV vehicles.

$$M_{fcm} = 23.544 P_{fc}^{0.508} \quad (2)$$

$$M_{H_2} = 0.0784 M_{tank} - 0.7721 \quad (3)$$

$$C_{battery}^{BEV} = 0.220 M_{battery}^{BEV} \quad (4)$$

$$C_{battery}^{FCEV} = 0.269 M_{battery}^{FCEV} \quad (5)$$

Where P_{fc} represents the power of the new system in kW, and M_{fcm} the mass of the fuel cell system module in kg. M_{H2} and M_{tank} correspond to the mass of hydrogen and the tank mass, respectively, both in kg. Additionally, $C_{battery}$ represents the battery capacity in kWh, and $M_{battery}$ the mass of the battery. Tables 2 and 3 present the estimated parameters for the FCEV, BEV and Range Extender.

Table 2: Estimated parameters for the FCEV and BEV conversion of the standard models

Vehicle	L6e	C - Segment	LD Van	E-Segment
Fuel Cell Power (kW)	6	80	90	-
Number of Cells	37	262	294	-
Active Cell Area (cm²)	200	375	375	-
Fuel Tank Capacity (kg)	1.0	4.3	4.5	-
Fuel Cell System Weight (kg)	71.8	218.1	226.5	-
Hydrogen Tank Weight (kg)	22.6	64.7	67.8	-
Battery Technology	Lithium-ion	Lithium-ion	Lithium-ion	Lithium-ion
Battery Capacity (kWh)	0.3	1.3	1.3	100

Battery Weight (kg)	11.2	48.3	48.3	454
Curb Weight (kg)	516	1583	1719	1904

Table 3: Estimated Parameters for the Range Extender Conversion of the standard models

Vehicle	L6e	C - Segment	LD Van	E-Segment
Fuel Cell Power (kW)	-	25	25	25
Number of Cells	-	82	82	82
Active Cell Area (cm^2)	-	375	375	375
Fuel Tank Capacity (kg)	-	1.8	1.8	1.8
Fuel Cell System Weight (kg)	-	120.8	120.8	120.8
Hydrogen Tank Weight (kg)	-	32.8	32.8	32.8
Battery Technology	-	Lithium-ion	Lithium-ion	Lithium-ion
Battery Capacity (kWh)	-	11	14	13.5
Battery Weight (kg)	-	125.1	77.8	61.4
Curb Weight (kg)	-	1529	1605	1666

For battery electric vehicles, no Eco, Boost, or Sport modes affecting SOC control were considered. The battery operates as the sole power source for the electric motor's demand, following a charge-depleting logic. For the control strategy of the fuel cell vehicles, was drawn from [18] for the E-Segment vehicle and linearly converted according to power to weight ratio of each vehicle in relation to the one in used in the study. For the Range Extender powertrain technology, the vehicle's propulsion primarily relies on the battery, with the fuel cell providing supplementary power to maintain the battery's state of charge and extend its range. This control will consist on CD- CS strategy. In charge-depleting mode, the vehicle operates as a BEV, relying solely on battery power. Once the battery's SOC drops below a certain threshold, the system switches to charge-sustaining mode. In this mode, the fuel cell provides power to maintain the battery's SOC within a narrow range. For this study, a minimum SOC threshold of 0.3 was chosen. The control of fuel cell power in charge-sustaining mode was implemented using a PID controller.

Energy consumption was estimated at the battery level using AVL CRUISE M software, which facilitates this by calculating the energy balance within the battery, accounting for both incoming and outgoing energy. Similar to the analysis at the battery level, hydrogen consumption will be examined at the fuel cell level, allowing for an assessment of the quantity of hydrogen that has reacted. Then to allow comparison between the two values, the hydrogen mass will be multiplied by the lower heating value (LHV) of hydrogen.

Both BEV and FCEV technologies are evaluated in HRH and HORH scenarios, while FCEVRx is not used. For passenger usage profile the L6e, C-Segment and E-segment are tested. Each model and technology is evaluated across all four scenarios (HRH, HORH, ARH, and AORH), with exception of the L6e model that is only tested with BEV and FCEV technologies. Only the LD Van model is tested for cargo usage

4 Results & discussion

4.1 Model Validation

To validate the developed vehicle models, a comparison of consumption values was conducted by testing the models under standard driving cycles specific to each vehicle type. For the BEV base standard driving cycle tests were conducted and compared accordingly with the manufacturer's published consumption values. The LD Van was tested under the WLTP Class 3b procedure, the L6e vehicle under the WMTC Class 1 procedure, and the C-segment vehicle using the NEDC cycle, as at the time the WLTP was not implement. Although numerous assumptions were incorporated in constructing the models with a large number of component parameters generated from the software tool, allied to hypothesis regarding adjustment of motor curves and efficiency maps, the results for the test cycles remained fairly consistent, aligning well with the published data and demonstrating

reasonable accuracy, as shown in Table 4. For the validation of the developed FCEV base model, consumption results and SOC evolution, as well as fuel cell, battery and electric motor parameters were compared against the reference control model used in this work, present in Table 5 as well as experimental results from the Argonne National Laboratory [18].

Table 4: Comparison of Energy Consumption of BEV vehicles: AVL Simulation Results vs. Published Data

AVL Cruise Model	Test Cycle	Declared Value	Simulation Value	Deviation (%)
L6e	WMTC Class 1	8 kWh/100km	8 kWh/100km	< 1
C-Segment	NEDC	15.0 kWh/100km	14.8 kWh/100km	1.33
LD Van	WLTP Class 3b	19.2 kWh/100km	19.4 kWh/100km	1.03

Table 5: E-Segment FCEV WLTP driving cycle results and comparison against experimental data

	AVL Model	Usmanov Model	Argonne Experimental
Hydrogen Consumption (g)	197.9	197.7	196.8
Relative Error to Experimental (%)	0.56	0.46	-
SOC (%)	63.2	63.3	62.5
Relative Error to Experimental (%)	1.12	1.28	-

4.2 Usage and Vehicle Technology scenarios

4.2.1 Passenger Vehicles

One of the first insights denotes that between all technologies within the same vehicle segment, considering the 4 routes, both for in RH or ORH, the ones that make use of a fuel cell, both FCEV and the FCEVRx in charging sustaining mode, show a considerably higher MJ/km values concerning the BEV and FCEVRx in charge depleting mode. Figure 1 shows the energy consumption for the Human-Driven Vehicles in route A1, A2,B1 and B2.

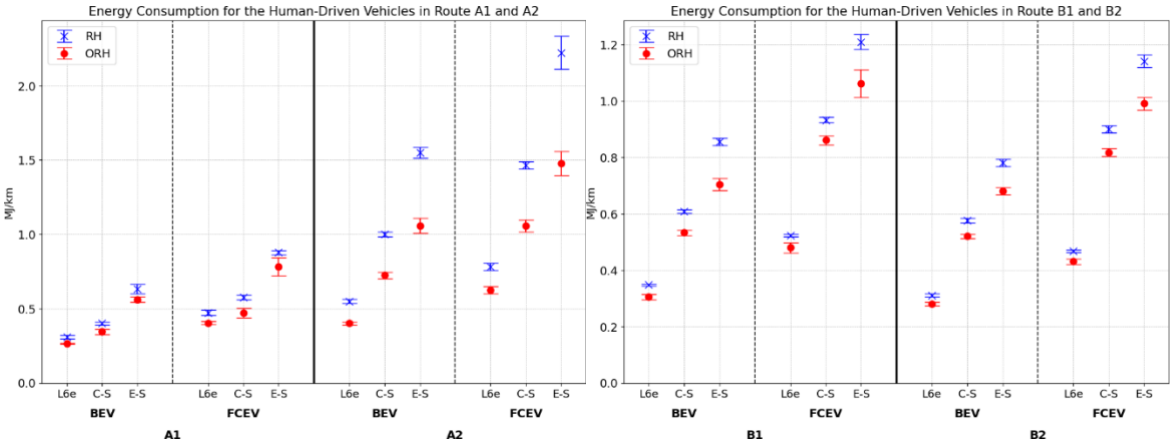

Figure 1: Energy Consumption for the Human-Driven Vehicles in Route A1,A2, B1 and B2.

From Figure 1 it is possible to observe that within Route A1, there is a slight difference between RH and ORH trips in each vehicle segment, even though the trip characteristics are fairly similar, with only a slightly higher number of stops for ORH (an average of two additional stops). During rush hour, however, stoppage time is significantly higher, leading to increased consumption for auxiliary systems. Additionally, the total percentage of time spent in acceleration and deceleration is slightly lower in the RH trip, suggesting that trip fluidity has a substantial influence on final consumption results. In contrast, Route A2 shows a more pronounced difference between ORH and RH, with RH having almost four times the number of stops, five times the stoppage time, and an acceleration and deceleration time percentage around half that of ORH. Notably, the influence of Δh in an ascending route further contributes to a significant consumption value increase relative to its counterpart. A

distinct pattern of increasing disparity between ORH and HR in consumption, as the vehicle model's power and weight increase is noticeable, contrasting with Route A1, where the gap only shows a slightly increasing tendency. When comparing the results of Routes B1 and B2, it is evident that the behavior and range of consumption values are fairly similar. This similarity relates to the routes' comparable nature regarding acceleration and stoppage patterns, although B1 shows less fluidity. Between B1 and B2, there is no pronounced Δh, and although Route B1 has a slight negative gradient, it shows higher consumption values than the respective B2 counterparts. This difference can be attributed to B1's reduced trip fluidity, while having an average of 7 more stops in HR compared to B2, where the difference in consumption values is also more evident. In ORH, however, the difference is less than 2 stops, and despite the acceleration and deceleration percentage difference between B1 and B2 being in line with HR values, the results are not that far apart, suggesting significant relevance regarding total movement stops, with Δh possibly also contributing to consumption increase and improve similarity. In this case, the observable increasing tendency as the vehicle segment rises, as seen in Route A2, is also noteworthy and is mirrored between the two routes. Concerning the FCEVRx in charge-depleting mode compared to the BEV, the results show that mass is the principal variable in action, as expected. The C-Segment FCEVRx is marginally heavier (8 kg) and consequently shows a minimal increase in comparison. For the E-Segment, the mass difference favors the FCEVRx as the lighter vehicle.

Regarding FCEV vehicle models the same trends in consumption are verified. The evolution of standard deviation is also similar, with special emphasis on the increase in deviation as the segment progresses. When comparing the consumption values of FCEVs and FCEVRx configurations, the FCEVRx generally shows higher energy consumption in all cases except one. This is despite the FCEV being considerably heavier — by approximately 50 kg in one case and 200 kg in another, the reason lies in the operational efficiency of the fuel cells: in the FCEVRx, the smaller fuel cell often operates closer to its maximum power output, where efficiency tends to decrease, while the full-size fuel cell in the FCEV typically operates within a more efficient region of the fuel cell efficiency curve, resulting in lower overall consumption. The only situation where this relationship did not prevail was for the E-Segment FCEV, which revealed worse performance for route A2 during RH, which, as discussed earlier, is especially prone to high consumption. This seemingly suggests that for this case the substantial vehicle mass, compared to the FCEVRx, offsets the efficiency advantage.

4.2.2 **Cargo Vehicles**

Results concerning the simulation of the cargo usage profiles are present in Figure 2.

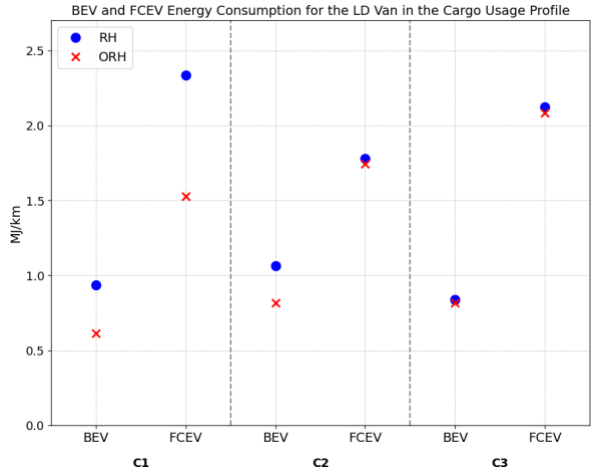

Figure 2: BEV and FCEV Energy Consumption for the LD Van in the Cargo Usage Profile

Starting with the two cargo routes (C2 and C3), where the fully loaded vehicle mode has its cargo gradually reduced, the results aligned with the previously discussed implications related to route characteristics. For C3 in RH, despite a 10% reduction in acceleration and deceleration times, less time

was spent stopped, thereby minimizing auxiliary consumption compared to the ORH case. Regarding stops, HR shows 9 more stops than ORH (44 versus 35), supporting the previously observed correlation in passenger scenarios between reduced movement fluidity and increased consumption values. However, since RH and ORH do not exhibit very pronounced differences in their characteristics, the consumption values remain fairly close. Examining the results for route C2 reveals a divergence in behavior compared to the previous route. This divergence is evident not only in the nature of the RH and ORH trips but also in the marked difference in trip fluidity. Specifically, the total number of stops more than doubled (137 versus 62), with over five times the stoppage time. Consequently, there is a reduction in acceleration and deceleration time percentage by 20% and 15%, respectively. Regarding the Δh_{max} the difference is more pronounced in C2 with 97 m when compared with C3 with 75 m, while both having a positive route gradient.

In the BEV case, results follow formerly discussed relations, however results in FCEV not only show results closely together, but looking at ORH results for C2 and C3 in the BEV technology, whose rounded value is by occasion the same, does not follow the tendency of showing much greater consumption values for C2 in relation to the ORH, and on the contrary values are closer than in the C3 scenario, which had a much more similar route nature. This divergent trend may be attributed to the regenerative braking system. The FCEV control strategy modulates the use of the battery and the fuel cell according to the State of Charge (SOC). When the SOC remains above 57%, the battery takes on a higher load, reducing the fuel cell's demand. The increased number of stops on route C2 also leads to more regenerative braking events, which may charge the battery above this threshold, thereby reducing the fuel cell power demand and hydrogen consumption. This may explain the similarity of RH and ORH values for the FCEV scenario in case 2 due to energy recuperation compensation as although C3 has slightly higher trip fluidity, the doubled number of stops in C2 may offset this difference through regenerative braking events. This suggests that regenerative braking in a loaded vehicle may be overly advantageous, contributing to a reduction in fuel cell demand. Finally, route C1 represents an unladen return for route C2. Both RH and ORH exhibit the lowest fluidity compared to their counterparts on the other routes and show the lowest Δh_{max}, though only slightly lower than C3 (with 73 m). The BEV technology results are fairly consistent with expectations based on previous BEV cases. Additionally, it benefits from carrying no load, which, combined with these conditions, contributes to lower consumption values, resulting in the best performance of all the aforementioned cases. Regarding the FCEV technology, the ORH case aligns with was verified for the BEV. Despite this, RH corresponds to biggest consumption quantity of all routes. An analysis of the consumption impact according to load nature for C2 and C3 was also performed. The BEV consumption shows an expected relationship between gradual load reduction and a constant maximum load, with the maximum load scenario having higher consumption values in all scenarios. It also provides insight that the average load underestimates all cases of gradual load, suggesting that the higher consumption impact during the initial moments of the route, when the load is greater than the average, offsets the effect of having a consistently lower cargo weight from the beginning of the trip. Meanwhile, the FCEV shows distinct behavior, with Max Load and Medium Load almost equal in C2 and Gradual Load and Medium Load partially aligned in C3. Referring back to previously discussed relationships, one can attribute in C3 that, with a higher vehicle mass, the more frequent complete stops in RH contribute to energy recuperation compared to the ORH case, offsets partially the superior cargo load as the route nature in RH and ORH is not far apart. While for C3 RH and ORH show a more marked distinction, and despite the higher number of stops, the increase cargo mass seems to stand prominent over regenerative braking compensation.

4.2.3 **Autonomous Passenger Vehicle**

A noticeable similarity between RH and ORH consumption values stands out, resulting from the highly similar nature of these two cases across all characteristics. The difference in the number of stops is minimal, remaining under 2 for A1, A2, and B2, with B1 being the exception, showing an increase of 6 stops compared to the ORH case. Additionally, the percentage of time spent in acceleration and

deceleration varies by no more than 2%. A decreasing trend in the gap between the highest and lowest technology consumption within the same vehicle also appears to emerge, particularly favoring the FCEV and FCEVRx in CS. This can be attributed to the nature of the driving cycle, which involves fewer stops and more cruising time at a near-constant velocity. As a result, fuel cell performance remains, for most of the time, in a higher efficiency region with minimal variation. As could be expected FCEVRx in charge depleting keeps the same trend when compared to BEVs as for the human-driven vehicle models, with mass being the only variable acting upon results. Figure 3 shows the energy consumption for the Autonomous Vehicles in route A1, A2, B1 and B2.

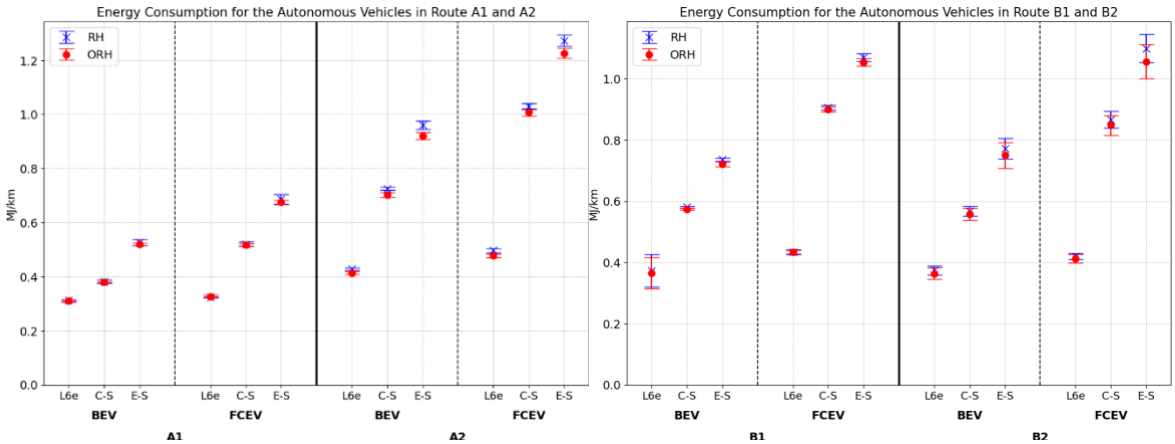

Figure 3: Energy Consumption for the Autonomous Vehicles in Route A1,A2, B1 and B2.

For route A1, the L6e shows BEV consumption in ARH and AORH levels comparable to the HRH. This suggests that despite a considerable improvement in fluidity, the increase in mass and much higher auxiliary power consumption (≈ 350% more) offset that advantage. Regarding FCEV energy use, results are significantly lower than in the HRH and HORH scenarios, which may, as discussed above, derive from increased fluidity of movement and operation in higher efficiency regions. Notably, in the FCEV, the AORH shows a very thinly higher value, which could be related to a phenomenon addressed in the previous section: with two very similar trips, having two additional stops enhances regenerative braking events and reduces fuel cell power demand. For the C-Segment, BEV consumption sits slightly above the average between HRH and HORH, suggesting that as the vehicle segment increases, the automation scenario starts to be more favorable in energy usage when relative to the human-driven scenario, with the E-segment having both cases being lower than the HORH. This same pattern is also verified for the FCEVs, sitting on a medium value of HRH and ORH for the C-Segment, and a considerably lower value than HORH for the E-Segment. Contrary to the last route, A2 consumption values in ARH and AORH tend to be in line with or below the respective HORH cases. A2 represented the highest energy expense for the passenger profile, showcasing very low movement fluidity in HRH. Examining ARH and AORH route characteristics, which show a significant fluidity increase over HORH with an almost 20% increase in time spent accelerating and decelerating, negligible stoppage time, and half the total trip time, the increase in auxiliary power and mass increment related to sensors achieves equilibrium for BEV technology in L6e (although with slightly higher consumption than HRH). The energy use values fall below the HRH level as the vehicle segment progresses, again suggesting that automation is more advantageous for heavier and more powerful vehicles.

Results suggest that, in general, the fluidity increase did not make the automation scenario more favorable. Examining the L6e data shows that although the advantage still holds for the FCEV, for the BEV technology's energy consumption values are above those of the HRH scenario. This indicates for the latter technology that the mass increment and auxiliary power demand relative to the L6e's base properties, five-folding the auxiliary power and adding a 6% total mass increase, outweigh any fluidity advantages for this segment in these routes. For the C-Segment, BEV technology aligns closely with HRH values, while the E-Segment sustains the premise of automation advantage, showing values

in line with HORH for these routes. Regarding FCEV technology the same pattern is verified with C-Segment values nearing HRH, while E-segment figures stay closer to the HORH cases.

5 Conclusions

This work provides insight into energy consumption values for passenger and cargo usage profiles in a real-world scenario, applied to the city of Lisbon, offering a comparative baseline across different technologies. In this work, MJ/km values for representative routes were determined for human- driven and autonomous vehicles during and outside of rush hour, presenting a qualitative comparison of energy consumption for various technologies, considering factors associated with representative routes and their specific characteristics. Traffic fluidity—with a particular emphasis on parameters such as the number of stops, stoppage time, and altitude act as a key factor influencing energy consumption. BEVs and FCEVRx demonstrated the lowest consumption values in MJ/km within each segment, with vehicle mass being the main differentiator between them. FCEVs and FCEV-Rx models displayed discrepancies due to variations in fuel cell efficiency, as the FCEVRx often operates in less efficient regions of the fuel cell efficiency curve. For cargo transport, insights were gained on the effect of regenerative braking in fully loaded FCEV vehicles, with frequent stops helping to offset the reduced route fluidity when comparing RH and ORH scenarios. Meanwhile, BEVs exhibited similar behavioral patterns to passenger vehicles. Further analysis also revealed the effects of different load scenarios, with BEVs again following consistent behavior and FCEVs showing divergent patterns. Conclusions were also drawn regarding automation potential and the comparison to conventional human-driven RH and OHR scenarios, indicating that higher car segments—those that are heavier and more powerful—benefit the most in terms of energy consumption reduction under automation.

This study faces some limitations. Firstly, it relies on a significant number of software-generated parameters to characterize vehicle behavior due to a lack of publicly available data. The feasibility of an FCEV L6e remains uncertain, as no geometrical or mechanical analysis was performed to ensure powertrain fit. Thus, the study offers only a conceptual view of potential consumption for this vehicle type. Assumptions in adapting technologies across vehicles may limit optimization. Control strategies for FCEV and FCEV-Rx models were derived from the E-Segment vehicle, possibly leading to suboptimal control. The FCEV-Rx uses a PID controller with a fixed SOC target, which could benefit from more advanced strategies to enhance fuel cell efficiency. Finally, software limitations affected the L6e's adherence to driving cycle speeds more than other vehicle segments. Regarding the driving cycle generation some deviations in total distance were noticed, although of no compromise as this study aim is to determine MJ/km values for the routes.

Acknowledgments

The authors gratefully acknowledge Fundação para a Ciência e Tecnologia for funding this research through the following programs: IN+ Strategic Project (1801P.00962.1.01 - IN+ UIDP/EEA/50009/2020 - IST-ID) and grant UI/BD/153621/2022.

The authors also acknowledge the Project BE.Neutral – Agenda de Mobilidade para a neutralidade carbónica nas cidades, contract number 35, funded by the Resilience and Recovery Plan (PRR) through the European Union under the Next Generation EU.

The authors gratefully acknowledge AVL, in collaboration with Instituto Superior Técnico, for providing the software utilized in this study and for their valuable technical support throughout the research process.

References

[1] United Nations. Goal 13: Climate Action, Accessed 2024. Accessed: 2024-03-17.

[2] United Nations Framework Convention on Cli- mate Change (UNFCCC). The paris agreement, n.d.

[3] United Nations Environment Programme (UNEP). Emissions Gap Report 2023. Online, 2023. Accessed: March 23, 2024.

[4] Hannah Ritchie, Pablo Rosado, and Max Roser. Emissions by sector: where do green- house gases come from? Our World in Data, 2020. https://ourworldindata.org/emissions- by-sector.

[5] European Commission, Directorate-General for Mobility and Transport. EU transport in fig- ures – Statistical pocketbook 2023. Publications Office of the European Union, 2023.

[6] Danyang Sun, Fabien Leurent, and Xiaoyan Xie. Discovering vehicle usage patterns on the basis of daily mobility profiles derived from floating car data. Transportation Letters, 13:163–171, 2021.

[7] Dingsong Cui, Zhenpo Wang, Peng Liu, Shuo Wang, Zhaosheng Zhang, David G. Dorrell, and Xiaohui Li. Battery electric vehicle usage pattern analysis driven by massive real-world data. Energy, 250, 7 2022.

[8] Jiaman Wu, Siobhan Powell, Yanyan Xu, Ram Rajagopal, and Marta C. Gonzalez. Planning charging stations for 2050 to support flexible electric vehicle demand considering individual mobility patterns. Cell Reports Sustainability, 1(1):100006, 2024.

[9] Danyang Sun, Fabien Leurent, and Xiaoyan Xie. Floating car data mining: Identifying vehicle types on the basis of daily usage pat- terns. volume 47, pages 147–154. Elsevier B.V., 2020.

[10] Chung-Hong Lee and Chih-Hung Wu. Learn- ing to recognize driving patterns for collectively characterizing electric vehicle driving behaviors. International Journal of Automotive Technology, 20:1263–1276, 2019.

[11] B. G. Pretorius, J. M. Strauss, and M. J. Booysen. Grid and mobility interdependence in the eventual electrification of operational minibus taxis in cities in sub-saharan africa. Energy for Sustainable Development, 79, 4 2024.

[12] Chris Martin Vertgewall, Marc Trageser, Mar- cel Kurth, and Andreas Ulbig. Modeling probabilistic driving and charging profiles of commercial electric vehicles. Electric Power Systems Research, 212, 11 2022.

[13] João David Monteiro Nunes. Avaliação do Desempenho Energético e Ambiental de Tecnologias Alternativas de Veíıculos a Partir da Criação de Perfis de Velocidade Representativos. Master's thesis, December 2021.

[14] Pedro Rodrigues, Ana Martins, Sofia Kalakou, and Filipe Moura. Spatiotemporal variation of taxi demand. In Transportation Research Procedia, volume 47, pages 664–671. Elsevier B.V., 2020.

[15] Helder Duarte and Cabral De Lima. Ur- ban logistics operations using electric mobility: Case study in lisbon, portugal mechanical engineering, 2017.

[16] Mohamed Ali Emam. A new empirical formula for calculating vehicles' frontal area. 2011.

[17] T. Burress. Benchmarking state-of-the-art technologies. In Proceedings of the Oak Ridge National Laboratory (ORNL), 2013 US DOE Hydrogen and Fuel Cells Program and Vehicle Technologies Program Annual Merit Review and Peer Evaluation Meeting, Washington, DC, USA, 14–16 May 2013.

[18] Umidjon Usmanov. Control strategy optimization of toyota mirai based fuel cell hybrid electric vehicles. Electronic, Politecnico di Torino, Corso di laurea magistrale in Automotive Engineering (Ingegneria Dell'Autoveicolo), 2022. Rel. Andrea Tonoli, Sanjarbek Ruzimov.

[19] J.M. Desantes, R. Novella, B. Pla, and M. Lopez-Juarez. Impact of fuel cell range extender powertrain design on greenhouse gases and nox emissions in automotive applications. Applied Energy, 302:117526, 2021.

[20] Ballard Power Systems. Fuel cell motive modules. https://www.ballard.com/fuel-cell- solutions/fuel-cell-power-products/motive- modules, 2024. Accessed: 2024-09-03.

[21] Toyota Motor Corporation. Fuel cell technology. https://www.toyota.co.jp/fuelcells/en/technology.html, 2024. Accessed: 2024-09-03.

[22] Toyota Motor Corporation. Toyota mirai technical specifications. https://media.toyota.co.uk/wpcontent/uploads/sites/5/pdf/210426M-NG-Mirai-Tech-Spec.pdf, 2021. Accessed:2024-09-30.

Presenter Biography

António Luciano is a M.Sc. student in Mechanical Engineering at Instituto Superior Técnico, Portugal. He developed his M.Sc. thesis work on the energy evaluation of alternative propulsion technologies in passenger and cargo light-duty vehicles, considering both human-driven and autonomous scenarios.

Miguel Campino received the M.Sc Degree in Mechanical Engineering (2021) from Instituto Superior de Engenharia de Lisboa. He is currently enrolled in the LARSyS PhD Programme focus on Sustainable Energy Systems. In his master thesis, developed in the area of transportation, Miguel focused on the propulsion management of a plug-in hybrid vehicle, developing a metric capable of bridge the gap between the test cycles under real conditions of use though forecasting methods. As a PhD student, Miguel is working to assess the real impacts of using light and heavy-duty vehicles with one or more propulsion sources at multiple levels.

Patrícia Baptista received the Ph.D. in Sustainable Energy Systems (2011) from Instituto Superior Técnico, Portugal. She is currently a Principal Researcher at IN+ Center for Innovation, Technology and Policy Research. Her main research topics have been on the quantification of energy and environmental impacts of alternative transport options, on how to influence user behavior by using ICT to characterize driving behavior and policy design for more sustainable transports.

Gonçalo Duarte received the Ph.D. in Mechanical Engineering (2013) from Instituto Superior Técnico, Portugal. He is currently Lecturer at Instituto Superior de Engenharia de Lisboa and Assistant Researcher at IN+ Center for Innovation, Technology and Policy Research. His main research topics address the real-world, on-road energy and environmental impacts of vehicle propulsion technologies, with particular focus on current and future vehicle certification standards and proceedings.